UNIVERSITY OF CALIFORNIA

Santa Barbara

Characterization and Comparison of Two Organic Mixed Ion-Electron Conductors

A Thesis submitted in partial satisfaction of the

requirements for the degree Master of Science

in Materials Science

by

Amanda Mikail Matheson

Committee in charge:

Professor Michael Chabinyc, Co-Chair

Professor Rachel Segalman, Co-Chair

Professor Kunal Mukherjee

June 2020

The thesis of Amanda Mikail Matheson is approved.

_____
Kunal Mukherjee

_____
Rachel Segalman, Co-Chair

_____
Michael Chabinyc, Co-Chair

March 2020

Characterization and Comparison of Two Organic Mixed Ion-Electron Conductors

by

Amanda Mikail Matheson

ABSTRACT

Characterization and Comparison of Two Organic Mixed Ion-Electron Conductors

by

Amanda Mikail Matheson

Semiconducting polymers, notably mixed ion electron conductors, have great promise for flexible and lightweight wearable devices that could integrate biology to electronics. The mechanisms for conduction in these materials are yet not fully understood, complicating the optimization of these materials for relevant applications. Here, we study two such polymers, poly(3,4-dioxythiophene-ethylene glycol) (ProDOT) and poly(thiophene-tetraethylene glycol) (P($g_4$2T-T)), using characterization methods including UV-visible spectroscopy, DC conductivity and electrochemical impedance spectroscopy, grazing incidence wide angle x-ray spectroscopy, and mass uptake of water and dopant. Both of the polymers redshift upon doping, and develop polarons of similar energies. Due to their slightly different structures, the two polymers exhibit different structural changes and mixed ionic-electronic conduction upon doping. Future work will include a more complete comparison of the two polymers to develop an understanding of the role of side chain concentration and position along the backbone in ionic and electronic conduction and morphology.

TABLE OF CONTENTS

LIST OF FIGURES

Introduction

One of the hallmarks of 21st century technology has been the development of wearable devices to monitor aspects of human health and to integrate technology with the human body. Wearable devices may soon have enhanced capabilities such as health monitoring, power generation, and sensing through the implementation of organic conducting polymers in such devices. Organic semiconductors already play a role in most electronic displays, and are responsible for the ubiquitous lightweight screens in televisions, laptops, and phones. The new technological forefront for organic semiconductors is mixed ion-electron conductors (MIECs).

Mixed ion electron conductors hold much promise for biointegrated technologies because they are capable of conducting both ionic and electronic currents, much like biological beings transmit chemical and ionic signals. The rules governing mixed conductors differ from those that govern organic semiconductors, like those found in OLEDs. While organic electronic semiconductors generally perform better with higher crystallinity (polyaniline), MIECs demonstrate high electronic and ionic conduction despite low crystallinity[1–4]. As ions generally reside in the sidechain groups on mixed conductors, and holes are generally thought to move along the conjugated backbones of these polymers, the modes of ion and electron conduction in mixed conductors are at odds. Electron conduction benefits when the polymer exhibits higher crystallinity, and ionic conduction benefits when the polymer exhibits more amorphous regions. Implementing mixed conductors into real devices will require a better understanding and manipulation of the balance between ion and electron conduction, and will certainly change between applications.

Two ion-electron mixed conducting systems that we chose to study are poly(3,4-dioxythiophene-ethylene glycol) (ProDOT) and poly(thiophene-tetraethylene glycol) (P($g_4$2T-T)). Both of these systems have a conjugated polythiophene backbone, which allows electrons to delocalize along the backbone and conduct when charge carriers are liberated through doping. Both of these systems also have poly(ethylene glycol) (PEG) sidechains which impart solubility to the polymers as well as the ability to conduct ions. ProDOT contains two PEG sidechains per polythiophene unit, so the system is soluble in most solvents at room temperature[2]. Moreover, it is highly ionically conductive due to these solubilizing side chains. P($g_4$2T-T) has two PEG sidechains per three monomer units. Compared to ProDOT, it is less soluble, though it is still easily processable at room temperature. These polymers can both be vapor doped with small molecules to introduce both electronic charge carriers and ionic species into the polymer films.

An advantage of both of these polythiophene based polymers is the ability to have simultaneous mixed conduction of both ions and electrons. Though the ProDOT is expected to have much higher ionic conductivity due to the greater number of PEG sidechains, both polymers can exhibit ionic and electronic transport. Other features of interest are that both polymers tend to be hygroscopic, which can enhance ionic conductivity, and they have rigid polythiophene backbones, lending themselves to more ordered structures favorable to electronic transport (e.g. π-π stacking). These two polymers were chosen over other conventional systems of study, such as P3HT or PEDOT:PSS, due to mixed conduction properties, pure formulations, and clear channels for transport of different charged species. Moreover, these two polymers are expected to behave similarly due to their similar structure (shown in Figure 1).

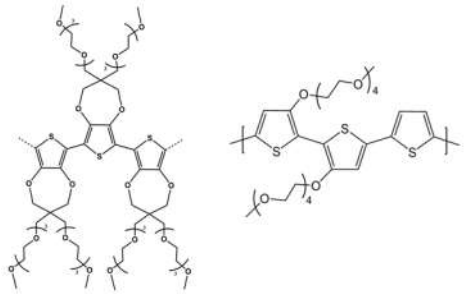

Figure 1: Chemical structures of ProDOT and P($g_4$2T-T).

This paper covers preliminary studies into the ion and electron conduction of ProDOT and P($g_4$2T-T). The main thrusts of study were to characterize the impacts of doping and humidity on the polymers, including: changes in the electronic structure (UV-Vis), changes in conductivity (DC and EIS), changes in physical structure and morphology (GIWAXS), and amount of dopant/water uptake (QCM). Detailed here are the sample preparation and procedures for each characterization method, as well as the results from characterization and a discussion of future work.

Methods and Sample preparation:

Grazing Incidence Wide Angle X-ray Scattering (GIWAXS)

Begin with a polished silicon wafer with either a thermal oxide layer or p-type doping. Cleave silicon into substrates approximately 14 mm x 14 mm in dimension so that they will fit in standard sample carrier cases. Clean substrates with a 5 min ultrasonication bath in acetone followed by an isopropanol rinse and 5 min ultrasonication bath in isopropanol. Dry each substrate with N_2 gun. This process removes particles on the silicon surface and cleans the silicon of any process residue. Shortly before spin casting, expose the samples to 4 mins of ozone in the UV-ozone (UVO) tool. The ozone reacts with and

removes organic molecules on the surface of the silicon. Once finished, spin cast polymer of interest onto silicon. Standard spin casting conditions are: 1000 RPM for 40 sec for a 20-100 nm film, depending on the polymer viscosity. After spin casting, anneal samples for 10 mins at 120 °C to evaporate off residual solvent and to improve film morphology. Dry samples overnight in ambient temperature high vacuum (10^{-8} Torr) oven. The high vacuum oven will remove water from the samples, allowing one to process them from a pristine state. Prepare samples as desired (including doping) prior to bringing them to a synchrotron source.

Humidity Measurement

Begin with a dried polymer sample on any substrate. Find the humidity chamber in the Segalman Lab AFM room or the Chabinyc Lab (set up only for quartz crystal microbalance (QCM) measurements). Both of the humidity chambers have a wet and a dry N_2 line—adjust the flow rates of each to adjust the humidity in the chamber. To access humidity above ambient, heat the water reservoir connected to the wet N_2 line. This may cause water to condense directly on the sample or in the humidity chamber.

Figure 2 below schematically represents the humidity and QCM setup in the Chabinyc lab. The QCM is sensitive to changes in mass, pressure, and temperature. This setup seeks to mitigate the pressure and temperature effects to singly measure mass changes. To use, turn on the dry N_2 line to a flow rate of about 2-3 ft^3/min. The initial flow rate is less important than having a constant flow rate throughout the experiment. Set the flow controllers (2 and 3 in the diagram) to the same max flow rate in order to prevent overpressure of the system. Set the 3 way mixing valve (1) to the desired ratio of N_2 diverted to the wet and dry line. Valve 1 has a type T port, which allows the dry N_2 line to be diverted only to the dry side,

the wet side, or to both simultaneously (Figure 2). Thus, pressure in the system can be kept constant while the ratio of wet to dry N_2 can be varied. To monitor humidity in real time, ensure the in-line humidity sensor is on and functioning. The sensor works fairly quickly, but takes approximately a minute to fully equilibrate to changes in humidity. As you turn the three way mixing valve, monitor the humidity sensor to access the desired humidity level.

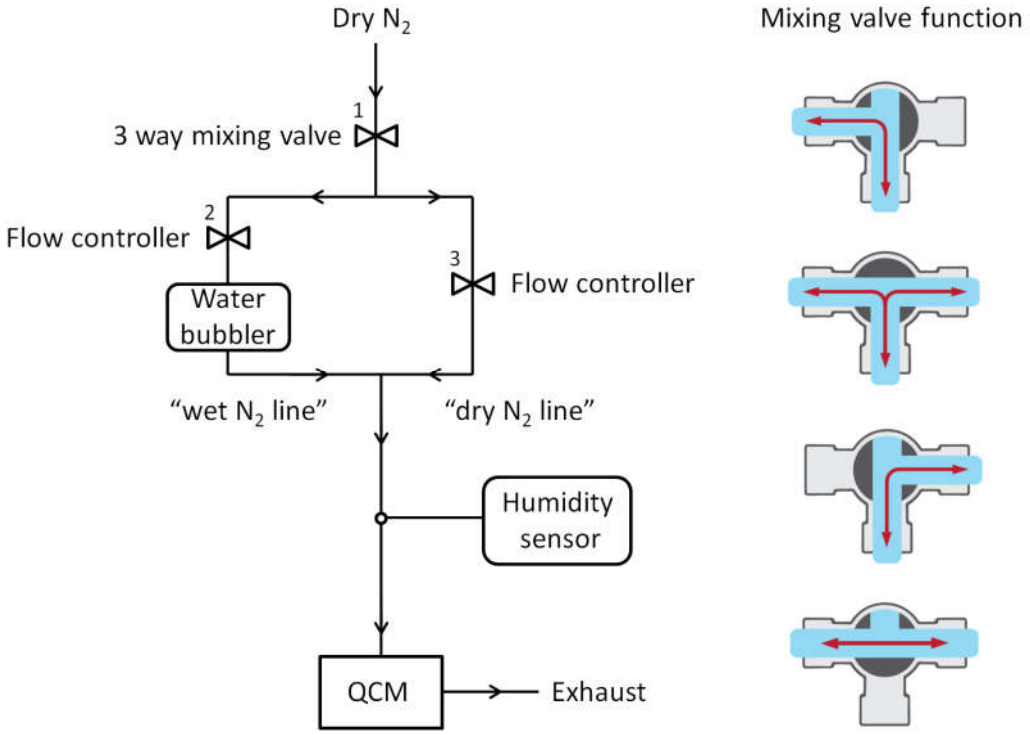

Figure 2: Schematic of static pressure humidity/QCM setup in Chabinyc lab (left). Schematic of 3 way valve function (Williams, 2018).

Vapor Doping

Always before handling dopants in the glovebox, wear large disposable gloves over the glovebox gloves to protect them from contamination. The vapor doping setup consists of a small jar (~ 60 mL) and a hotplate. Before doping, bring the small jar into a glovebox and pour in a small scoop (~1 mg) of the dopant molecule of interest. Place a piece of double sided tape on the inside of the jar lid. Bring the hotplate up to the doping temperature (Table

1). When the hotplate is at temperature, affix samples onto the tape (film side facing *away* from tape), screw the jar lid on, and place the jar on the hotplate for the desired doping time. When done, remove the jar from the hotplate and remove the samples from the lid. Post doping, you may choose to anneal the samples on the hotplate to remove excess dopant from the film. Post doping and cleanup, purge the glovebox to clean it of the small molecule dopant.

Table 1: List of common dopants and corresponding hotplate temperature settings.

Dopant	**Hotplate temperature**
HTFSI	25-60°C
F_4-TCNQ	200-210°C
$NOPF_6$	160°C

Quartz Crystal Microbalance (QCM)

Quartz crystals for the QCM should only be handled with plastic or plastic-tipped tweezers, to prevent scratching and chipping of the crystals. Before using a QCM crystal, all prior material on the crystal, such as polymer or dopant, should be removed. This is best done by thorough rinsing with solvents and time in the plasma cleaner. The cleaning protocol will depend on the polymer used on the crystal.

Starting with a clean quartz crystal, place the crystal in the UV-ozone chamber or plasma cleaner for 4 mins. Blow off any dust with a nitrogen gun. Some polymer solutions, such as PEDOT:PSS, require a surface pretreatment to properly adhere to the substrate. For PEDOT:PSS, the typical protocol is to submerge the crystals in a 1mM solution of 11-mercapto-1-undecanol in ethanol for 2-12 hours, then blow dry with nitrogen[5]. Polymer solutions in polar solvents may also benefit from this surface treatment. After pretreating, spin cast or drop cast polymer solution onto the QCM crystal. Ensure the final film thickness is less than 1 μm; greater than that thickness and the QCM will not be able to attain

resonance with the crystal[6]. Spin casting in general will keep the film thin enough to be measured by the QCM. Anneal the films at 100-120°C for 10 mins to dry off residual solvent. If there is polymer deposited on either of the gold contacts on the backside of the QCM crystal, wipe off the polymer using a cotton-tipped applicator saturated with solvent. If the polymer is not wiped off, the crystal will not make good electrical contact with the QCM. If desired, place the crystals under high vacuum (~10^{-8} Torr) for 12 or more hours to ensure a very dry film. Store the crystals in a dry glovebox until use.

Surface Treatments

If a polymer is not casting well onto a substrate, dewets from the substrate surface, or does not form a uniform film, a surface treatment may be necessary to improve the adhesion between the polymer and the substrate. In the table below, common surface treatments for different substrates, as well as their protocols, are described. The surface treatments described below are all self-assembled monolayers (SAMs) which alter the substrate chemistry to improve polymer wetting and adhesion. Deposit polymer on substrates shortly after doing the surface treatment to ensure maximal adhesion.

Table 2: Common SAM surface treatments for certain substrates and their corresponding procedures.

Surface Treatment	Substrate	Procedure
Silanization:		
HMDS Hexamethyldisilazane (vapor-prime)	Glass, quartz, metal-oxides, silicon	In a fume hood: - Bake substrate at 110 °C for 10 mins to evaporate water off surface - Prepare a clean petri dish (lid + bottom) to evaporate HMDS - Place substrate in petri dish - Pipette a ~100 µL drop of HMDS into petri dish, off to the side of the substrate

		- Close petri dish lid and let sit for 5 mins - Remove substrate, blow off excess HMDS with N_2 gun - Clean petri dish with solvent and dry
OTS Octadecyltrichlorosilane	Glass, quartz, metal-oxides, silicon	In a fume hood: - Place substrate in UVO for 4 mins - Mix 1 mM OTS-Toluene solution in a small beaker (up to 10 mM is fine) - Rinse substrate with acetone and IPA - Submerge substrate in OTS solution for 5 mins - Dry substrate with N_2 gun - Dispose of OTS solution
Thiolization:		
11-mercapto-1-undecanol[5]	Gold	In a fume hood: - Place substrate in UVO for 4 mins - Mix 1 mM 11-mercapto-1-undecanol in ethanol in an appropriately sized beaker or petri dish - Submerge substrate in thiol solution for 2-12 hours, covering beaker/petri dish with foil to block light from entering - Remove substrate and dry with N_2 gun - Dispose of thiol solution

Electrochemical Impedance Spectroscopy (EIS)

An EIS measurement is an electrochemical impedance measurement of a polymer film. An AC voltage signal is inputted into the film, and the resulting output AC signal is measured. For polymer thin films, the AC signal is swept from 3 MHz to 1 Hz at a V_{pp} of 10 mV. Higher V_{pp} may lead to degradation or damage of the film. EIS may be conducted in a number of geometries, though for thin polymer films it has been found that the interdigitated electrodes (IDEs) work well, as they reduce the likelihood of a short circuit occurring. Moreover, the films on IDEs can be nano-thin, which conserves material and enhances interfacial effects which may impact ion transport. The IDEs must be used with thin films (<1 μm), as the electric field radiates elliptically from the electrodes and is complicated to model for films thicker than the inter-electrode spacing[7]. Sample preparation for EIS is the

same as for GIWAXS, though using the interdigitated electrodes (IDEs) rather than blank silicon as the substrate.

Following the SOP for the EIS instrument, initialize a measurement scanning from 3 MHz-1 Hz at V_{pp} = 10 mV. Place the voltage probe tips on the large rectangular gold pads on the IDEs. To ensure good contact between the probe tips and the gold pads, it may be necessary to scrape away some of the polymer on the pads if it is covering the pads. The IDEs have a thermal oxide layer in contact with the polymer and gold pads, so the substrate does not have to be grounded. Run the measurement, being sure not to touch the EIS setup. Below, Figure 3 illustrates a qualitative example of what pure electronic and mixed ionic-electronic conduction will look like on a Nyquist Impedance curve, with sample equivalent circuits suggested for that mode of conduction.

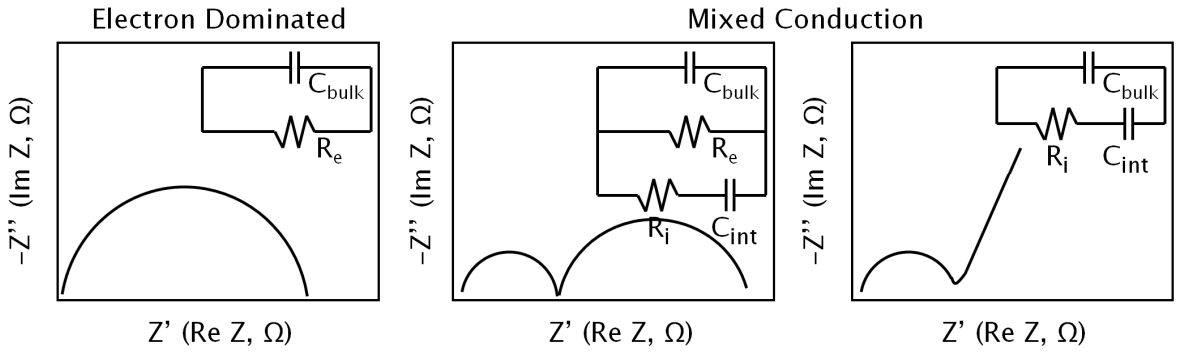

Figure 3: Example qualitative EIS Nyquist Impedance curves. Mixed conduction may manifest as either of the rightmost curves, and electronic conduction will manifest as the left curve. Sample equivalent circuits given.

Interdigitated Electrodes (IDEs)

The process steps for making the IDEs are summarized in the table below. Use N-doped silicon with a ~ 200 nm thermal oxide layer as the substrate for IDEs. Due to the robust metal contacts, the IDEs may be reused. If reusing, ensure that the previous polymer

has been totally removed from the IDE surface. A combination of ultrasonication in solvent and plasma cleaning may be necessary to fully remove the previous polymer. IDE mask pattern provided by the Patel group at the University of Chicago.

Table 3: Steps for the fabrication of IDEs.

Step	Description
Cleaning	Rinse silicon wafer with acetone, methanol, and isopropanol for ~ 30 seconds each. Substrates may also be cleaned in acetone, methanol, and isopropanol baths in an ultrasonicator. Dry wafer with N_2 gun.
Prebake	Bake wafer at 110 °C for 10 min to evaporate residual solvent and water to improve HMDS prime.
HMDS prime	Place wafer on spin coater and soak surface completely with HMDS. Spin wafer to dry. RPM: 3000, Ramp: 500 RPM/s, Time: 35 s.
Spin cast resist	Spin cast ~ 50 mL AZnLOF 2020 resist on wafer. RPM: 3000, Ramp: 500 RPM/s, Time: 35 s. Will make a ~ 2.1 μm thick film.
Prebake	Set wafer on 110 °C hotplate for 90 s.
Expose	Using the IDE mask, align substrate and mask in Karl Suss MA-6 mask aligner (9 mW/cm² at 365 nm). Expose for 6 s.
Postbake	Set wafer on 110 °C hotplate for 60 s to crosslink resist.
Develop	Submerge exposed wafer in ~ 500 mL MIF 300 for 60 s, gently agitating or swishing the wafer the whole time. Rinse twice in ~ 500 mL DI water or with DI water gun and dry with N_2 gun.
Descum	In RIE tool, flow oxygen at 300 mT, using 100 W power for 30 s. For RIE #5, use "O2 Flow", which has the settings: O_2 at 20 sccm, 100 W, 20 mTorr, for 40 s. RIE #5 username: Chabinyc, password: chabinyc
Metal Deposition	In electron beam deposition source, deposit 5 nm Ti or Cr at 1.0 Å/s and 40 nm Au at 2 Å/s. Ti will not corrode in acidic environments, and is less likely than Cr to react with ionic species.
Liftoff	Submerge wafer in ~500 mL AZ n-methyl-2-pyyrolidone (NMP) rinse solution heated in an 80 °C water bath for 1-4 hours. Gently agitate wafer in solution until excess material is lifted off. Rinse with NMP, methanol, and isopropanol. Dry with N_2 gun.
Cleave	Cleave off IDEs as needed or pre-cut all of them with dicing saw.

UV Visible Spectroscopy

Clean quartz or glass substrates as described in the GIWAXS section. Spin or drop cast polymer solution onto substrate, typically with concentration between 2-10 mg/mL. Anneal the film for 10 minutes on a 120°C hotplate. Dope film if necessary. Perform UV-Vis as prescribed by SOP for the instrument.

DC Conductivity

Clean quartz or glass substrates as described in the GIWAXS section. Evaporate desired contacts directly onto substrates. A sample pattern mask is shown below in Figure 4. Using the desired pattern mask, evaporate 20-40 nm Au on the quartz or glass substrate. For more durable contacts, first evaporate a thin layer of Cr or Ti (~ 5 nm), then evaporate the 20-40 nm Au. Spin cast or drop cast the polymer solution on the substrate, then anneal the film for 10 mins on a 120°C hotplate. Dope the film if necessary.

The typical DC conductivity measurement is a transmission line measurement, in which the DC conductivity of the sample is measured between four or more points at different distances from each other. This allows the user to calculate the contact resistance between the voltage probes and the sample and to calculate the resistance of the film itself. Using one of the voltage probe stations, secure the sample to the base of the probe station. Place one voltage probe tip on one of the thin gold contacts, ensuring the tip is fully in contact with the gold layer under the polymer film. Place the other voltage probe tip on a nearby thin gold contact, again ensuring full contact. This measurement will be performed at least three times across four of the thin pads, as illustrated in Figure 4. As described in the SOP for the voltage probe station, run the DC conductivity measurement, recording the

resistance value measured by the probe station. Then, move one of the voltage probe tips onto the next thin gold contact, and perform the DC measurement at this new distance. Repeat the measurement for at least one more distance, and plot distance versus film resistance. A linear fit of the measured DC resistance values will elucidate the contact resistance (y-axis intercept) and the film resistance (slope).

The transmission line measurement requires that the interface between the contacts and the polymer film is ohmic, and that the contact between the voltage probe tips and the contacts is also ohmic. To improve the interface between the polymer and the contacts, match the work functions of the contact metal and the polymer as closely as possible. To test the contact between the gold pads and the voltage probe tips, place both voltage probe tips on the same gold pad and run the DC conductivity measurement. This should create a short circuit (0 V); however, if there is a non-negligible resistance measured, the metal contact/probe tip interface is not ohmic and the transmission line measurement will not yield accurate results.

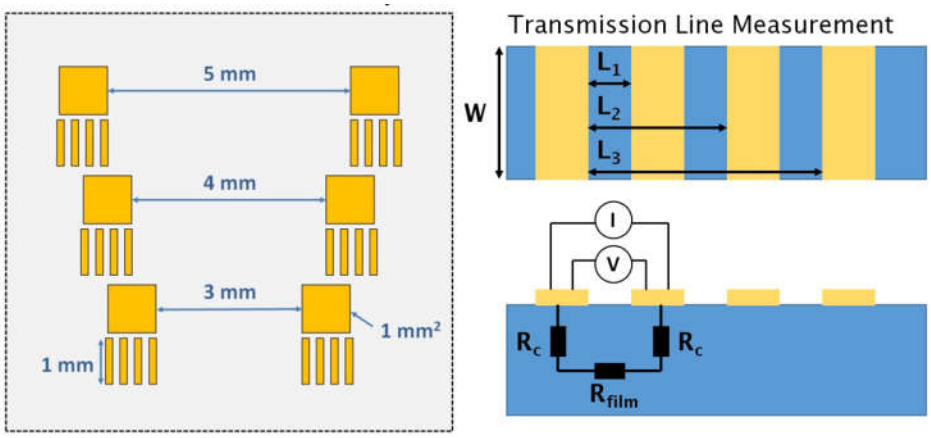

Figure 4 : Thermoelectrics mask with small thin pads used for TLM measurement (left). Schematic of TLM measurement (right).

Data collected and analysis

UV Visible Spectroscopy

UV Visible spectroscopy (UV-Vis) was utilized primarily to assess the doping state of the polymers post vapor doping with small molecules. The process of doping a polymer changes its electronic state such that charge carriers are introduced into the film and the HOMO and LUMO levels of the polymer are shifted through the charge transfer process. As many polythiophenes absorb in the visual range, the charge transfer and energy level shift modify the absorption spectrum of the polymer, resulting in a visible color change. Typically this manifests as a bleaching of the polymer and a redshift of the absorption spectra as the energy gap between the HOMO and LUMO levels decreases[2,8]. Up to a certain point, UV-Vis can indicate the doping level of a polymer. The longer the polymer is exposed to the dopant, the more dopant (by mass) enters the film and dopes the polymer, resulting in greater bleaching of the polymer. With certain molecular dopants such as F_4TCNQ, the actual doping state of the polymer can be measured by the area under the polaron peak and correlated to number of charges in the film[2]. In the case of colorless dopants such as HTFSI, we cannot access the number of molecules in the film via UV-Vis, though we can estimate when the film is fully doped by pushing the bleaching until completion.

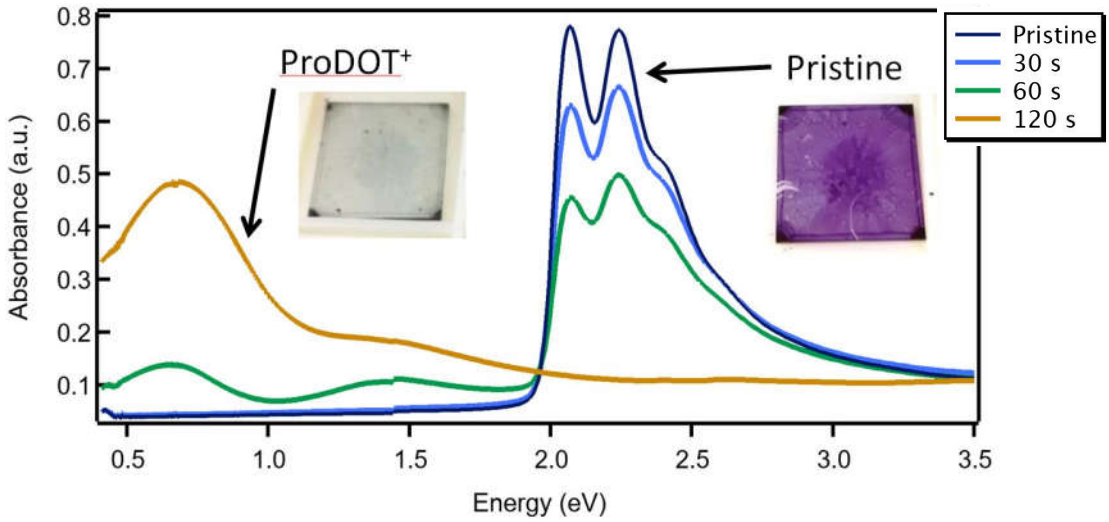

Figure 5: Doping of ProDOT thin films with HTFSI at 60 °C. Insets show visible bleaching of films upon exposure to dopant.

Figure 5 above illustrates the doping of ProDOT with HTFSI. The dark blue peaks between 2.0 and 2.5 eV are the signature peaks for ProDOT. As dopant is introduced, the intensity of these peaks decreases, until the polymer is nearly fully bleached. At high levels of dopant, the polaron peaks in the IR region become more prominent, indicating a greater proportion of free charge carriers in the polymer backbones. Inset in the UV-Vis plot are pictures of the pristine polymer film and the doped film. Notably, the pristine film absorbs strongly in the 2.0-2.5 eV region, while the doped film is nearly colorless.

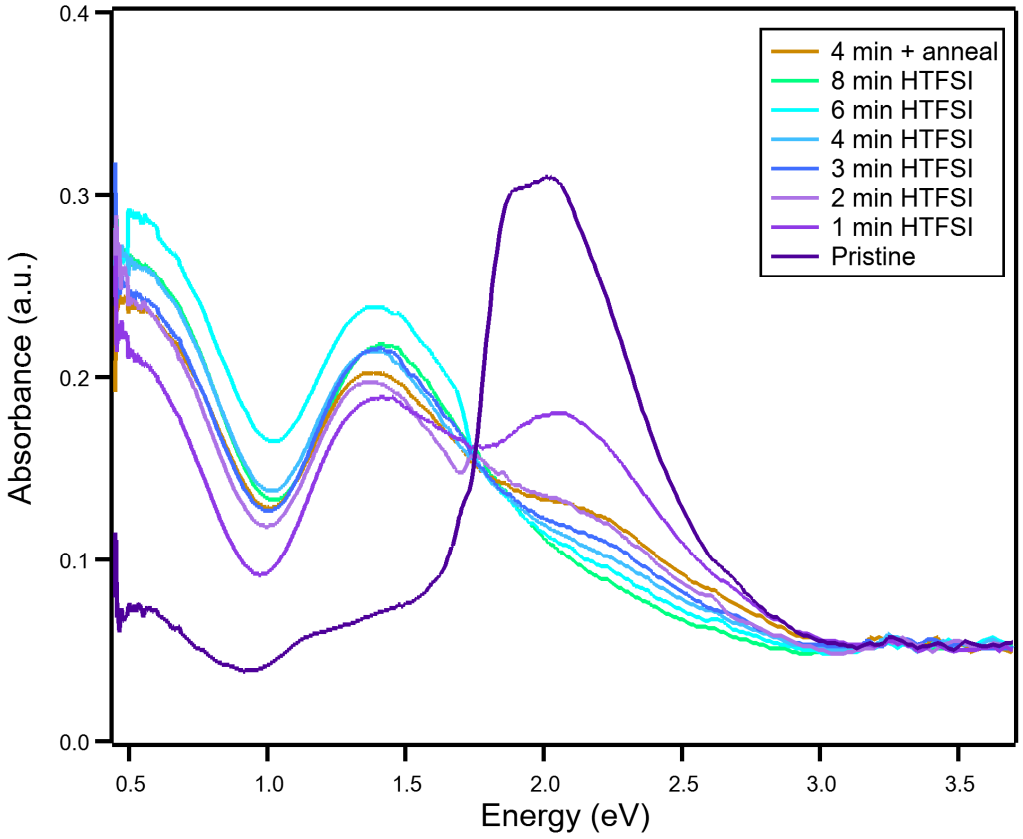

Figure 6: Doping series for P($g_4$2T-T) and HTFSI.

Similar to ProDOT, P($g_4$2T-T) absorbs strongly around 2.0 eV, giving it a dark purple/blue color. As the film is doped with HTFSI, the central peak sharply decreases in intensity and the film absorbs strongly in the IR region (Figure 6). There are some differences in doped spectra between the ProDOT and the P($g_4$2T-T). The P($g_4$2T-T) spectra demonstrates two polaron peaks, one centered at 1.4 eV and the other around 0.5 eV. ProDOT has one peak centered at 0.7 eV, and a weak absorbance peak at 1.4 eV. Both polymers dope quickly with HTFSI at room temperature, and it can be determined from the UV-Vis spectra of the doped P($g_4$2T-T) that longer doping times (after approximately 4 minutes) do not substantially improve doping of the polymer.

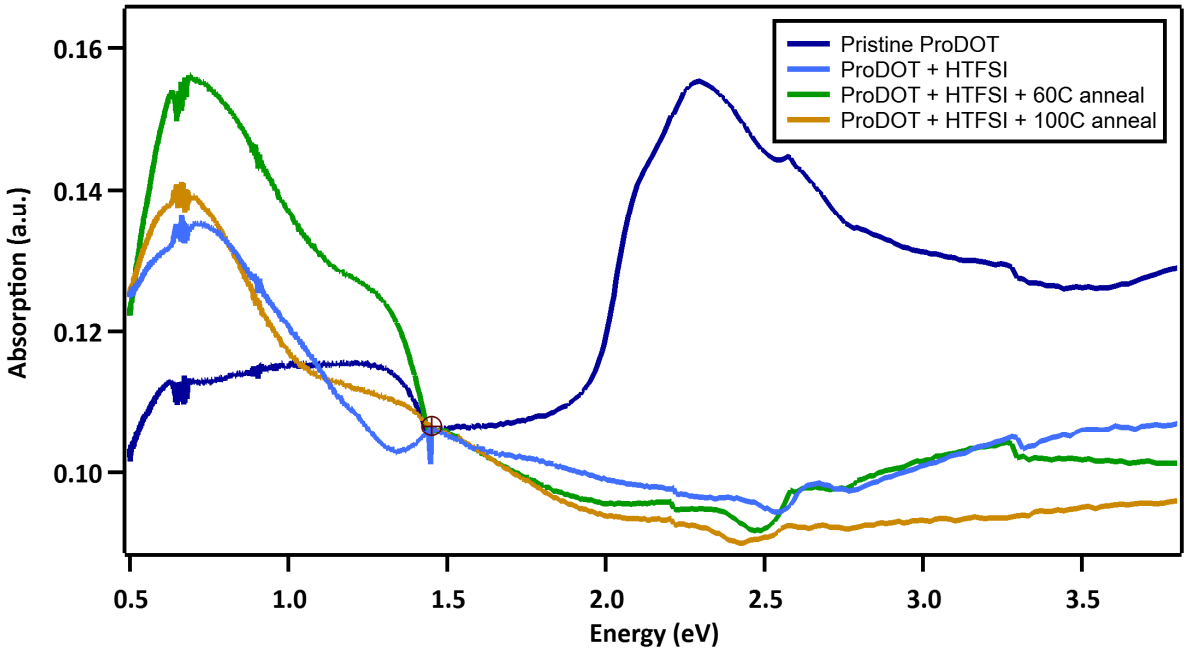

Figure 7: Effect of annealing on doping level of ProDOT with HTFSI.

Vapor doping polymers directly over the dopant molecule can cause the dopant to crystallize on the surface of the polymer. To remove the excess dopant, the polymer can be annealed on a hot plate and the excess dopant will evaporate off of the polymer surface. Post doping annealing may also enhance the doping of the film, as can be seen from the UV-vis spectra of ProDOT annealed at 60 °C (Figure 7). Likely, the added thermal energy in the film allows the dopant molecules to more easily diffuse into the film and dope the entirety of the film. Post-doping annealing does not reduce the doping of the film, even at higher temperatures (100 °C).

DC Conductivity

The DC conductivity of films was assessed with a transmission line measurement. Though the HTFSI-doped ProDOT films appeared to fully bleach, the DC conductivity was quite low compared to other doped polythiophenes like P3HT (P3HT vapor doped with

F_4TCNQ shows conductivities up to 48 S/cm)[9]. The conductivity plot below illustrates the measured conductivity of doped and pristine samples over time. Despite full doping, the average HTFSI doped ProDOT conductivity is $1.21*10^{-5}$ S/cm, a 100x improvement over the pristine conductivity, and putting the doped sample in the range of hundreds of MΩ of resistance (Figure 8). The low conductivities may be due to ions in the film inhibiting the flow of electrons at the gold electrodes. The low DC conductivity values motivated the use of EIS to measure the electronic and ionic conductivity of ProDOT.

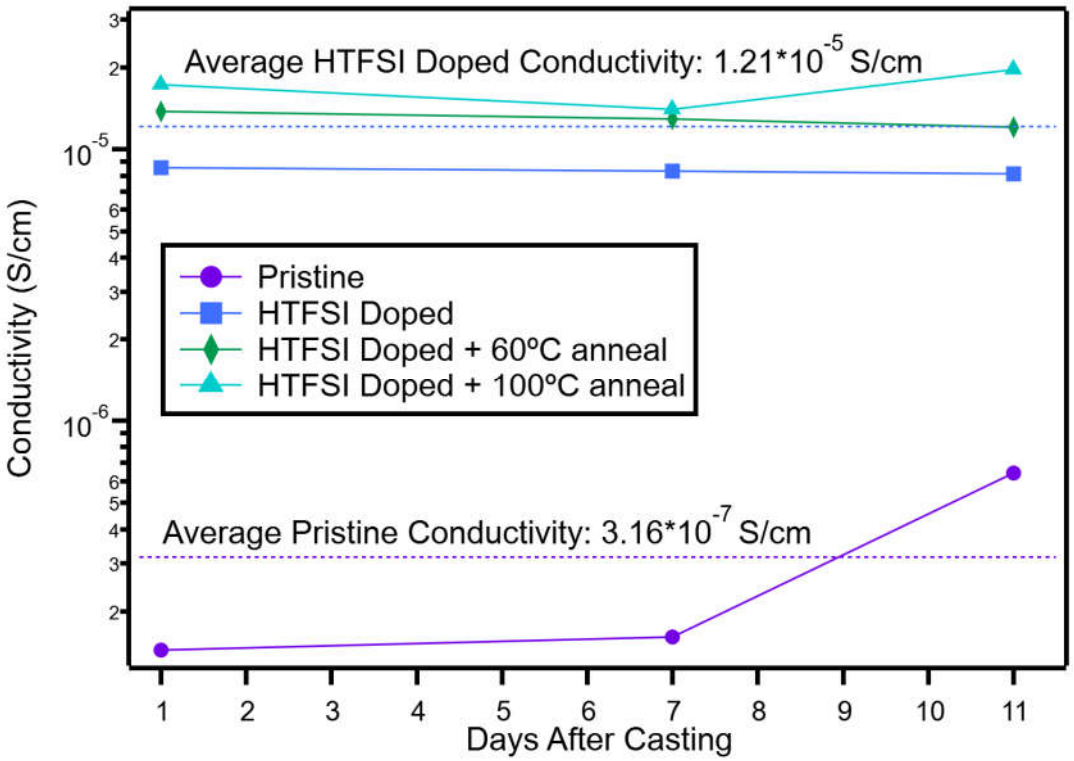

Figure 8: Poor DC conductivity of doped and pristine ProDOT films.

Electrochemical Impedance Spectroscopy (EIS)

The poor DC conductivity prompted the use of electrochemical impedance spectroscopy (EIS) to deconvolute the electronic and ionic conductivities of the film. Due to the small amounts of polymer material, measurements were conducted on substrates with

interdigitated electrodes (IDEs) provided by the Patel group at University of Chicago. EIS scans were run 7 MHz to 1 Hz with an applied voltage of 0.01 V.

For thin films (thickness h << electrode spacing d), the electronic conductivity of the film can be related to measured resistance via

$$\sigma = \frac{1}{R_{film}} \frac{d}{(N-1)lh} \quad (1)$$

where d is the electrode spacing, h is the thickness of the film, N is the number of interdigitated electrodes, and l is the length of the electrodes[7]. The IDEs used in this thesis have dimensions d = 8 μm, l = 3 mm, w = 2 μm, N = 480.

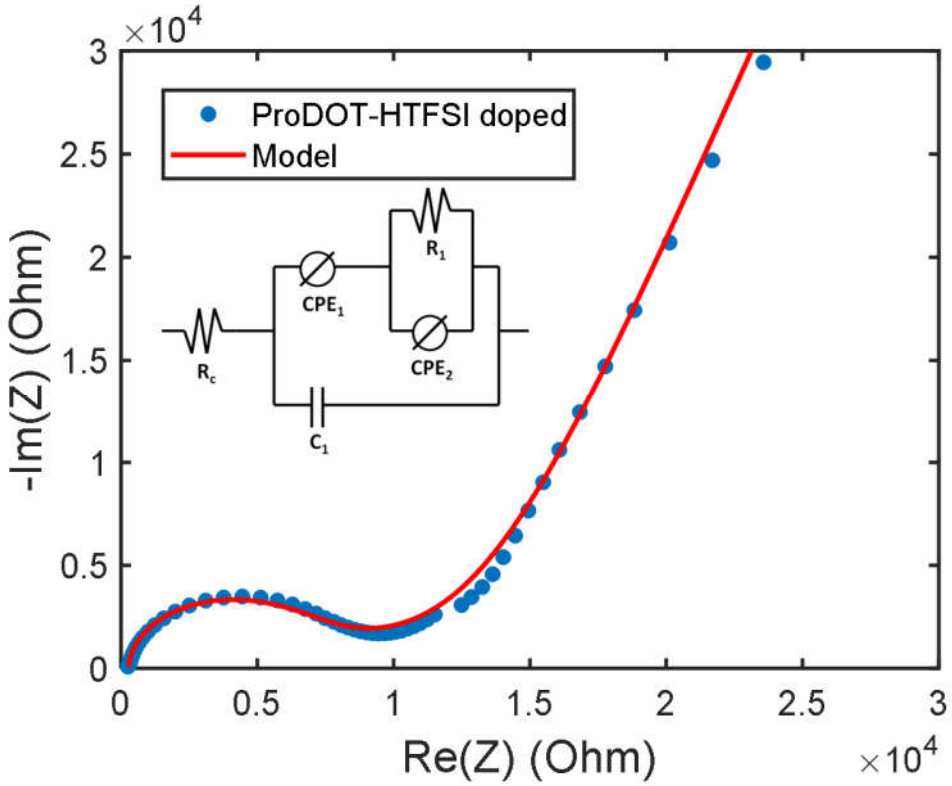

Figure 9: Nyquist plot of ProDOT fully doped with HTFSI. R_c = 286.9 Ohms; C_1 = 0.7408*10^-9 F; CPE_1 Q = 46.56*10^-6 F*s^(a-1), a = 0.0987; CPE_2 Q = 2.886*10^-6 F*s^(a-1), a = 0.8567; R_1 = 1.254*10^4 Ohms. R_c corresponds to the contact resistance and R_1 corresponds to the resistance of the film.

ProDOT fully doped with HTFSI demonstrates mixed conduction, indicated by the semicircle (electronic portion) and capacitive tail (ionic portion) in the Nyquist plot (Figure 9). The capacitive tail indicates that ions are trapped at the electrodes, inducing capacitance in the film[10]. The empirical fit shown in the plot above suggests non-linear capacitive processes. While we can be confident of the resistance fits, as they are verified by DC conductivity, the other circuit elements are more difficult to experimentally verify so this model must be taken with some skepticism. The film is highly resistive, indicating low electronic conduction. The conductivity of this film calculated from Eq. (1) is $1.16*10^{-4}$ S/cm.

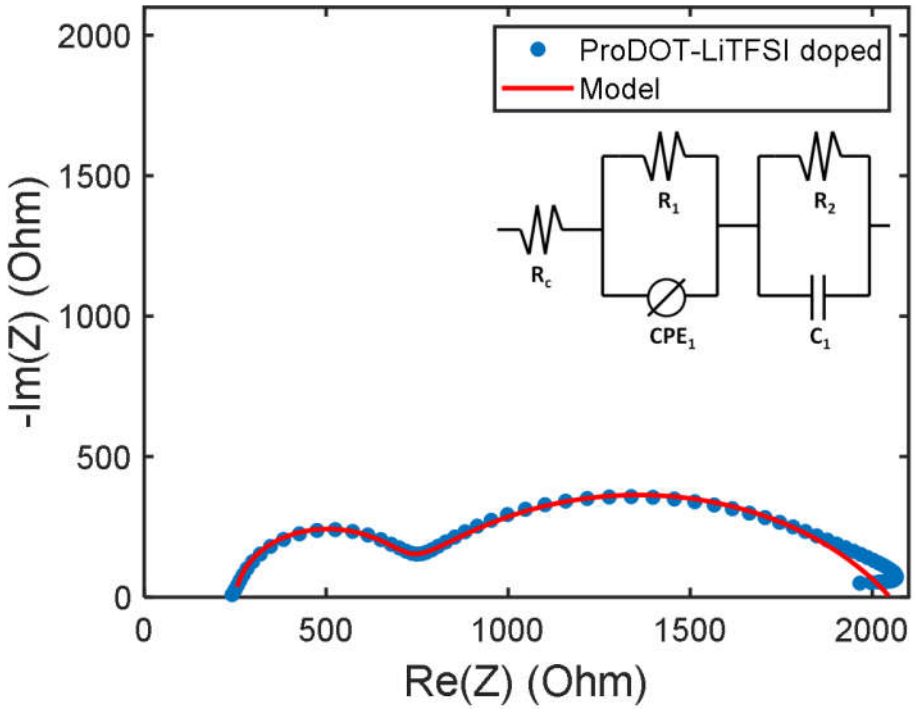

Figure 10: ProDOT fully doped in solution with LiTFSI. R_c = 249.3 Ohms; R_1 = 1375 Ohms; CPE_1 Q = 4.192*10^-06 F*s^(a-1), a = 0.6181; R_2 = 424.2 Ohms; C_1 = 1.714*10^-9 F.

ProDOT doped with LiTFSI also demonstrates mixed conduction, indicated by the two semicircles in Figure 10. The high frequency semicircle (left) corresponds to electronic

conduction, and the low frequency semicircle (right) corresponds to ionic conduction, as ions and electrons diffuse at different time scales due to their unique mobility in the polymer. Notably, the lack of a capacitive tail indicates that ions are not accumulating at the electrodes, blocking current flow. This may be because the kinetics of ion motion for the Li+ are faster than for TFSI-, so the lithium can move freely throughout the film without forming a capacitive double layer at the electrode-polymer interface. The electronic conductivity is given by the high frequency semicircle and R_2, and is 0.0033 S/cm.

Due to the low availability of ProDOT polymer, P($g_4$2T-T) was used as a substitute system to observe mixed conduction in polythiophenes. ProDOT and P($g_4$2T-T) share similar structure with a conjugated backbone and ethylene glycol sidechains; however, P($g_4$2T-T) has much fewer sidechains per monomer unit (0.66 sidechains/unit vs 2 sidechains/unit for ProDOT) and is thus less soluble than ProDOT in any solvent. Moreover, it is expected that the lower number of polar sidechains will bind fewer ions[11], meaning that the ionic conductivity will be lower in this polymer.

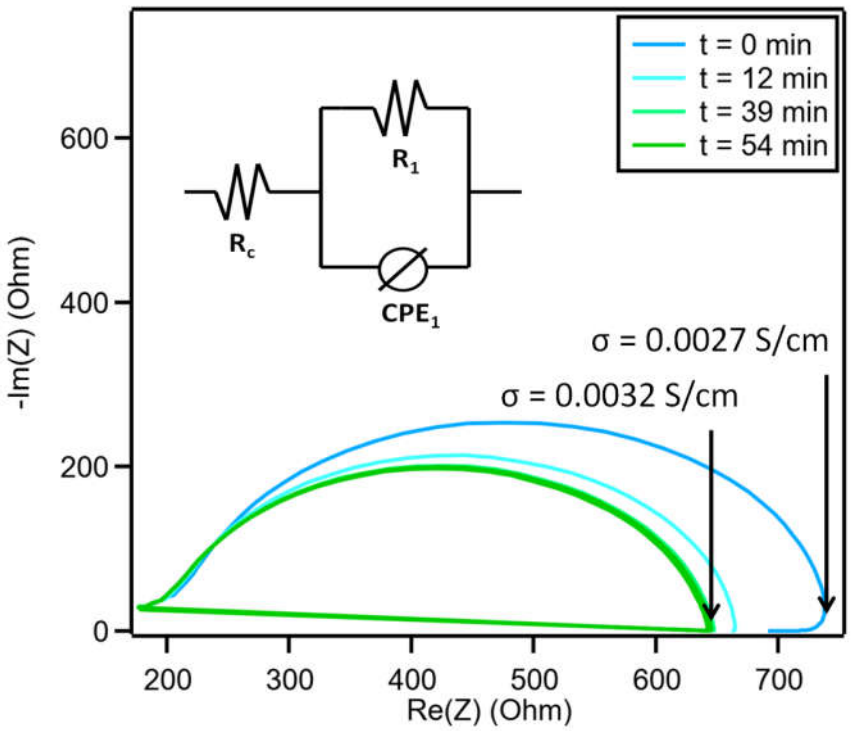

Figure 11: Increasing conductivity of pristine P($g_4$2T-T) upon exposure to air. Sample was initially dried in the high vacuum oven prior to measurement. Impedance model demonstrates only electronic conduction in the film.

Figure 11 above is a Nyquist plot from EIS conducted on pristine P($g_4$2T-T), tested in ambient conditions over the course of an hour after drying overnight in the high vacuum oven. As shown by Kroon *et al*[11], the polymer was observed to oxidize slightly in air, which improved doping conditions and conductivity. The improvements in conductivity likely derive from the polymer oxidizing in air, imparting improvements in conductivity without the presence of a dopant. The figure above illustrates a highly depressed semicircle, which can be attributed to a capacitance-like behavior deriving from slow diffusion-like processes[7] or non-uniform current through the polymer[12].

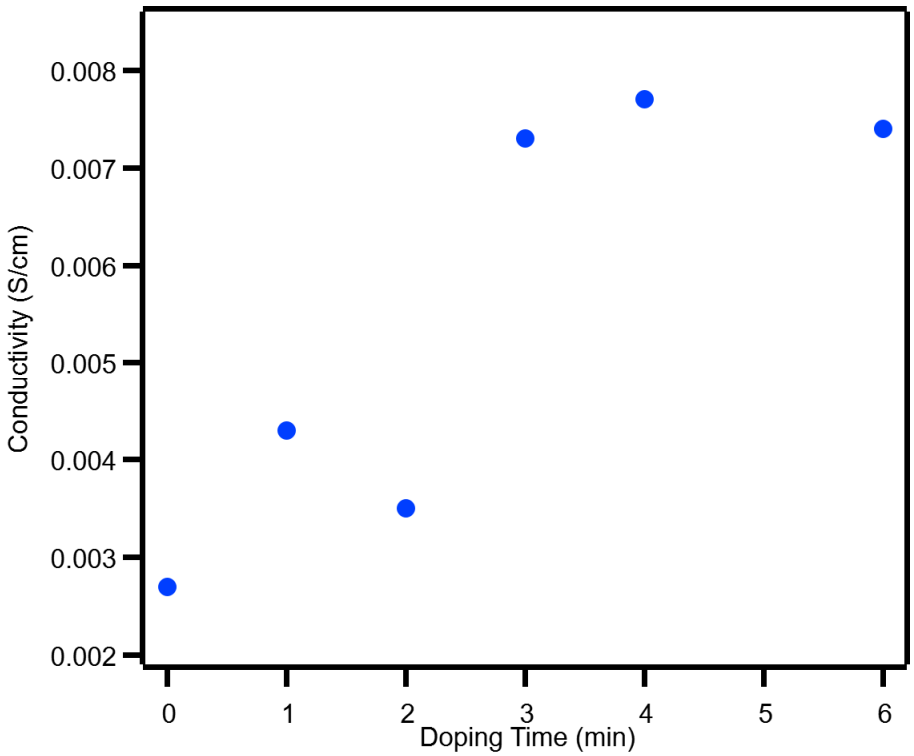

Figure 12: Measured conductivity of P($g_4$2T-T) films with increasing exposure to dopant. Notably, the electronic conductivity of P($g_4$2T-T) is much higher than ProDOT, even in the pristine case.

Figure 12 illustrates the conductivity of HTFSI vapor doped P($g_4$2T-T), with increasing exposure to dopant. The equivalent circuit for this system is the same as for the pristine P($g_4$2T-T) case, as the polymer either demonstrates negligible ionic conductivity or has an electronic signal that overwhelms the ionic. The pristine conductivity of this polymer is much higher than previous reported values (on the order of 10^{-5} S/cm[11,13]), suggesting that the polymer may be already oxidatively doped in the so-called pristine state. Moreover, the polymer does not access the high post-doping conductivities previously reported--up to 25 S/cm with F_4TCNQ dopant—even with the same dopant molecule HTFSI[11,13]. This polymer has likely doped in air, resulting in modest improvements to conductivity and a decreased ability to further dope upon the introduction of extra dopant molecules. This problem may be remedied by de-doping the polymer chemically.

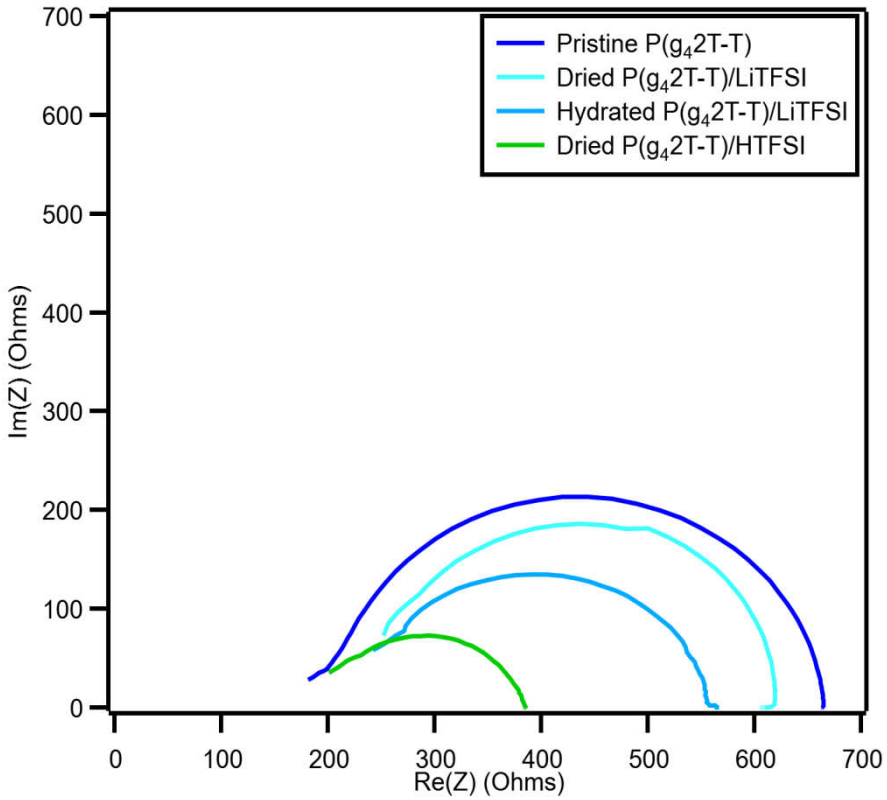

Figure 13: Comparison of HTFSI and LiTFSI-doped P($g_4$2T-T). Ionic conductivity is negligible for both dopants.

The HTFSI dopant both dopes the backbone of the polymer and leaves an ion in the sidechains, imparting both ionic and electronic conductivity. The ionic conductivity in this polymer is overwhelmed by the electronic conductivity, so it is not detectable with EIS. The polymer was also doped with LiTFSI, with the expectation that the Li would minimally dope the polymer backbone and that the Li+ and the TFSI- would both impart higher ionic conductivity to the polymer than the TFSI- alone. Even in humid conditions, where we expect the ionic conductivity to be highest[14], the ionic signal was still overwhelmed by the electronic signal in P($g_4$2T-T) (Figure 13). The LiTFSI electronically dopes the polymer minimally, as the doped polymer has a similar conductivity to the pristine polymer, while the HTFSI doped polymer experiences a ~ 3x improvement in conductivity. Compared to ProDOT, the ionic conductivity of P($g_4$2T-T) is very low, likely due to the fewer number of

solubilizing side chains per monomer unit. To detect ionic conduction in this polymer, it may be necessary to use pulsed field gradient nuclear magnetic resonance imaging (PFG NMR), which could more closely track ion motion throughout the film.

Grazing Incidence Wide-Angle X-ray Scattering (GIWAXS)

GIWAXS is an x-ray scattering technique that probes length scales of ~5-30 nm by reflecting x-ray light at shallow angles (> 89.5°) relative to the normal direction of a thin film. This technique can be conducted on thin films to conserve material. GIWAXS yields information about both in plane (q_{xy}) and out of plane (q_z) packing of polymer chains. As conjugated polythiophenes with solubilizing side chains, both ProDOT and P($g_4$2T-T) are expected to have both crystalline and amorphous regions. Ions, including those from dopants like HTFSI and F_4TCNQ, as well as water molecules have finite volume and should disrupt the crystalline ordering of the polymer film in some way. GIWAXS can yield insight into the packing of these polymers, as well as the influence of hydration and dopant molecules on the structure of the polymer thin films. All of the intensity plots below were generated by integrating the intensity of the reflected light from q = 0.2 $Å^{-1}$ to q = 1.2 $Å^{-1}$, with an azimuthal angle extending from 2°-8° from the vertical direction (also known as a "cakeslice").

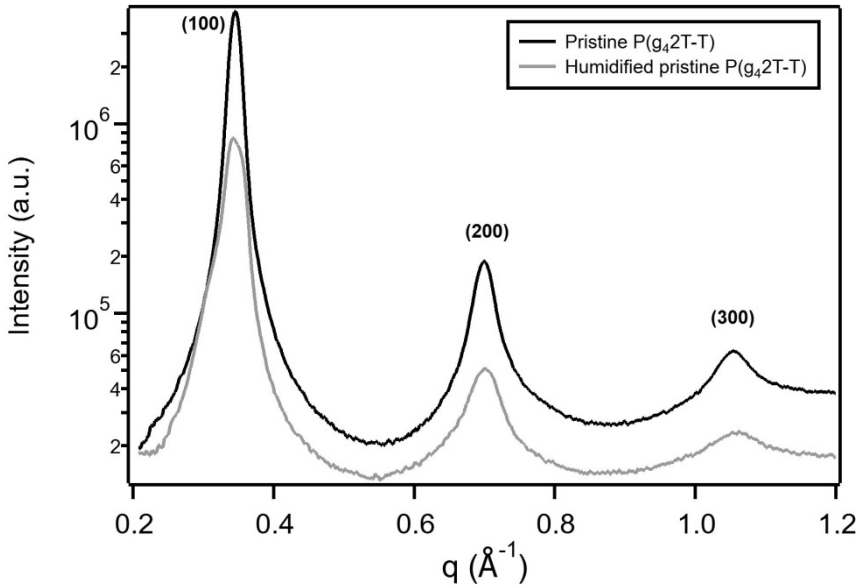

Figure 14: Comparison of the structure of dried and humidified pristine P($g_4$2T-T). Humidity in the film does not disrupt the unit cell size, though it does reduce the crystalline fraction of the film.

Pristine P($g_4$2T-T) exhibits molecular packing on the order of 5.95 nm. As illustrated in Figure 14, the introduction of water into the film does not change the location of the packing peaks in the film, indicating that water minimally disrupts the crystalline regions of P($g_4$2T-T) films. The introduction of water molecules may reduce the overall crystallinity of the film, as the intensity of those peaks decreases upon humidification. However, when both dopant molecules and water are introduced into the film, the packing of P($g_4$2T-T) changes drastically, and in fact behaves differently depending on the processing conditions. When the dopant HTFSI is added to the pristine dry film via vapor doping, the dopant molecules occupy space in between polymer chains, increasing the distance between polymer chains (Figure 15). The addition of water molecules via humid air after doping does not induce additional structural change to the film. However, when dopant molecules are introduced into a hydrated P($g_4$2T-T) film via vapor doping, almost all structure in the polymer film disappears, indicating a nominally amorphous film.

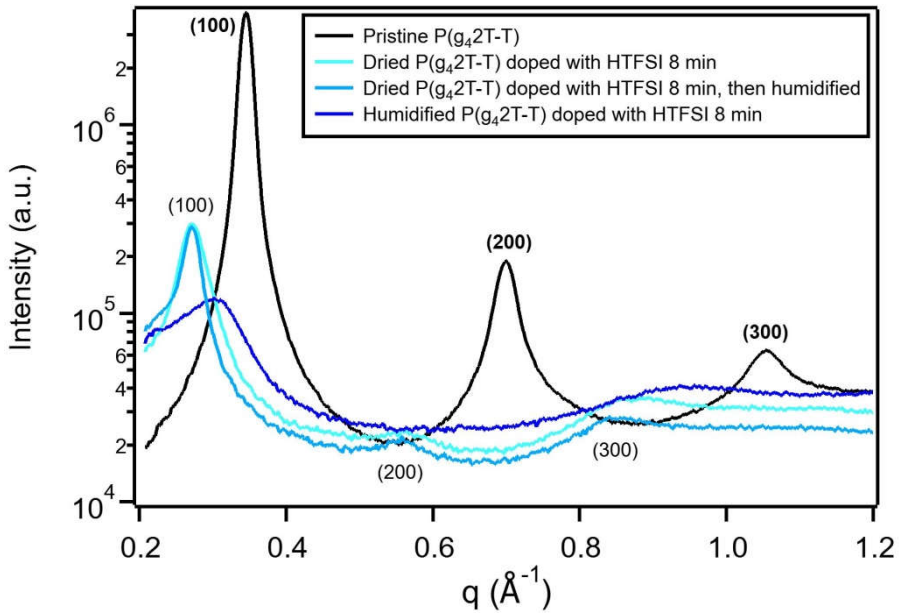

Figure 15: Effects of doping, humidity, and processing conditions on the crystalline ordering of P($g_4$2T-T).

Annealing enhances structural order induced by doping[13,15]. As noted in the UV-Vis section of this paper, a post-vapor doping anneal improved the degree of doping of the film, possibly by allowing dopant molecules to migrate within the film and dope the film to completion. Post-vapor doping annealing also enhances the structural changes induced by the addition of dopant to the film. Figure 16 illustrates both the greater definition of packing peaks in the film as well as the formation of a fourth order peak, indicating a strong reordering of the film induced by the dopant. The packing distance changes from 5.95 nm to 7.05 nm upon the introduction of HTFSI dopant. Moreover, a post-dope anneal intensified the peaks, indicating greater ordering, and initiated the formation of a fourth order peak, indicating longer range order in the film. The unit cell dimension decreases slightly from the vapor doped sample to the 100°C annealed sample. This may indicate the evaporation of excess dopant in the film, leaving the final unit cell more compact than in the vapor doped case.

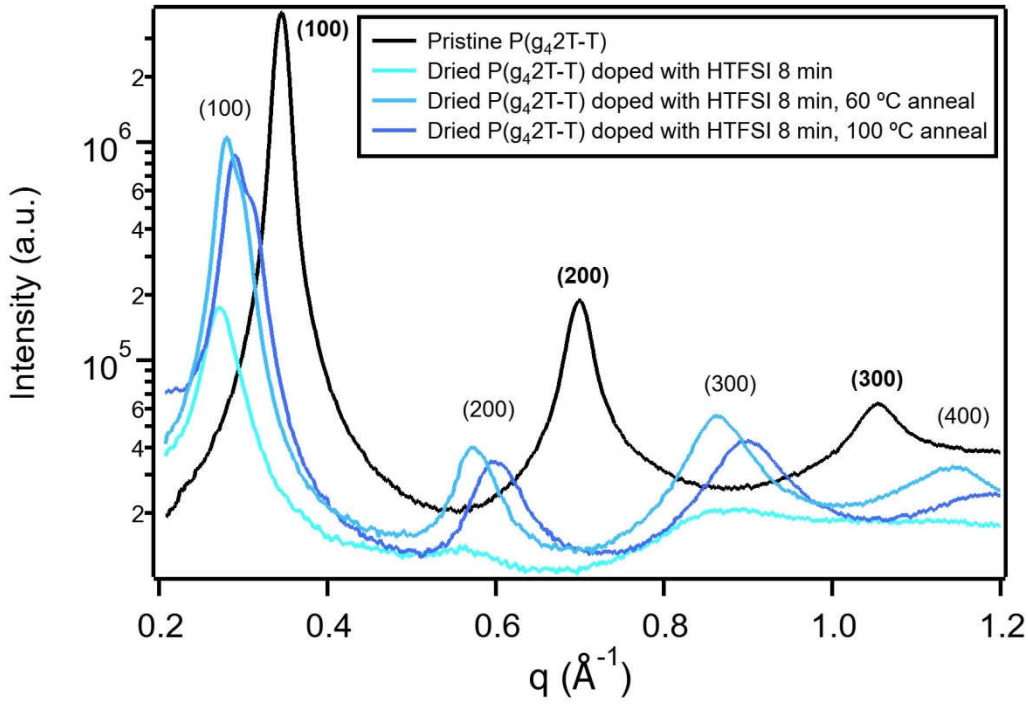

Figure 16: Post-vapor doping annealing enhances the structural changes induced by the dopant molecule.

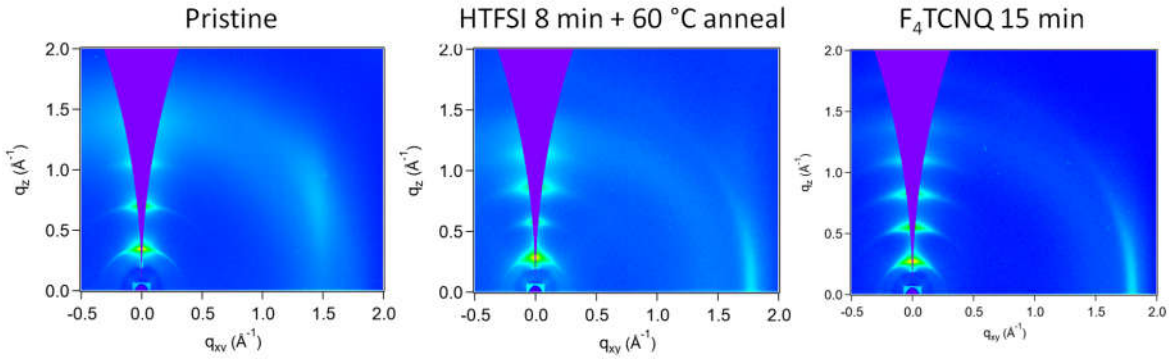

Figure 17: 2D GIWAXS patterns of P($g_4$2T-T) films doped with HTFSI and F_4TCNQ. Plots illustrate distinct alkyl ordering in the films, and weak π-π stacking.

Much of the reordering in the P($g_4$2T-T) film upon doping occurs in the q_z direction, which is associated with alkyl spacing between polymer chains (Figure 17). This is indicative of ions intercalating in the sidechains of the polymer and avoiding the conjugated backbone. Moreover, ions appear to enhance the alkyl ordering of the film, which may

facilitate ion conduction through the sidechains. This phenomenon occurs regardless of dopant used, and is in fact more pronounced upon the intercalation of larger dopant ions such as F_4TCNQ and $NOPF_6$ (Figure 17). Despite film reordering, the polymer does not conduct ions efficiently through the alkyl sidechains, as surmised from impedance spectroscopy. The strong alkyl ordering and weak π-π stacking in the film suggest other electronic conduction pathways than the usual π-π interactions between chains.

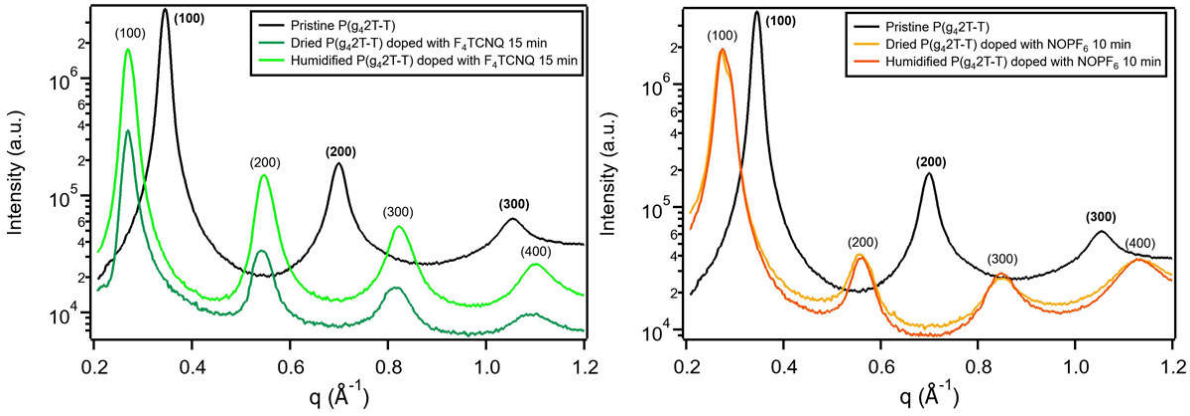

Figure 18: Changes in P($g_4$2T-T) film structure with F_4TCNQ and $NOPF_6$ dopants, in dry and humidified films. Both dopants induce greater structural ordering in the film, especially in the alkyl direction.

GIWAXS was also conducted on ProDOT films doped with HTFSI. Similar to the P($g_4$2T-T) films, HTFSI induces alkyl ordering in the film, especially with increasing concentration of dopant in the film (Figure 19). For higher doping times, the ProDOT film appears to develop structure, indicated by the regular spaced intense spots around 0.35 $Å^{-1}$. Peak fitting shows this nearly-hexagonal unit cell to have dimensions b = 20.2 nm and c = 27.9 nm, with the a-axis being indeterminate in this scattering geometry. The polymer chains may be organizing as hexagonally packed cylinders in the crystalline regions of the film. Lower dopant concentrations did not show this enhancement in polymer ordering upon doping.

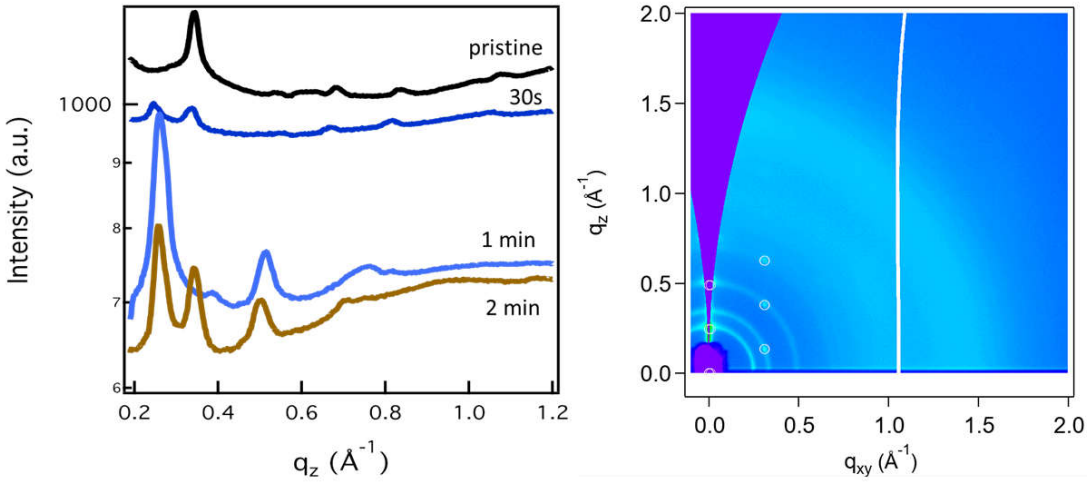

Figure 19: Left: ProDOT doped with HTFSI. Longer doping times increase the concentration of dopant in the film and induce greater alkyl ordering in the film. Right: ProDOT doped for 2 mins with HTFSI.

Quartz Crystal Microbalance (QCM) for humidity detection

The Gamry quartz crystal microbalance (QCM) with dissipation was purchased to measure the water and ion molecule uptake of polymer thin films such as P($g_4$2T-T). The QCM operates via the piezoelectric effect observed in quartz. When the crystal receives an electrical impulse, the crystal deforms, and when the impulse is released, the crystal returns to its original configuration. The QCM stimulates an AT-cut quartz crystal with an AC signal, causing it to resonate around 5 MHz. When the temperature of the crystal, the pressure applied to the crystal, or the mass of the crystal changes, the resonant frequency of the crystal changes, and is measureable down to tenths of Hz. The impedance response of the crystal is measured to observe changes to the resonant frequency. Notably, QCMs with dissipation also measure the harmonic resonant frequencies of the quartz crystal, allowing the user to measure changes in viscosity, in or out of a liquid.

The mass change of a quartz crystal is modelled by the Sauerbrey equation;

$$\Delta f_n = -2nf_1^2 \frac{\Delta m/A}{(\rho_q \mu_q)^{1/2}} \quad \text{(Hz)} \quad (2)$$

$$\Delta m/A = \frac{\Delta f_n (\rho_q \mu_q)^{1/2}}{-2nf_1^2} \quad \text{(ng/cm}^2\text{)} \quad (3)$$

where Δf_n is the change in frequency of the nth-harmonic (Hz), Δm is the change in mass of the crystal (g), A is the area of the crystal face (cm^2), ρ_q is the density of quartz (2.648 g/cm^3), and μ_q is the shear modulus of quartz (2.947x10^{11} g/cm·s^2)[6]. The correct application of this equation depends on the following assumptions: uniform film distribution on the quartz surface; good adhesion of the film to the surface; the film thickness is significantly less than the thickness of the crystal; and the film is a rigid layer, otherwise visco-elastic models are required to correctly calculate the mass change[6].

Initial studies of the water uptake of P($g_4$2T-T) revealed a number of issues with the humidity setup as well as with the thin film. The initial humidity setup had two separate nitrogen lines with separate flow control. One line was the dry nitrogen line, and the other was the wet line, and was routed through a bubbler filled with water to humidify the nitrogen. The flows mixed and then were sent to the QCM. This setup did not regulate pressure well in the system, so any changes to either the dry or wet line pressure changed the pressure of the entire system. This conflated changes in pressure with changes in humidity and generated inaccurate results. The setup also did not effectively humidify the nitrogen—maximum humidity levels hovered around 60 %. Additionally, the films of P($g_4$2T-T) were cast from a 6 mg/mL solution of P($g_4$2T-T) in chlorobenzene, and were cast at 1000 RPM. This resulted in films that were 20-30 nm thick. In addition to the flaws in the humidity setup, the films were not able to absorb much water due to their thinness.

To troubleshoot the system, we moved to thin films of PEDOT:PSS, as these films are water based and will therefore absorb water after drying. The QCM crystals were treated with a thiol SAM before spin casting Clevios PH1000 at 2000-3000 RPM and drying overnight in the high vacuum oven. Here, it was found that too thick of films are also problematic with the QCM. The maximum load on a crystal is limited by the total damping of the crystal and lost sensitivity[6]. Thick films contribute to both of these problems, and it was found that a PEDOT:PSS film on the order of a micron thick would cause the crystals to lose resonance and be unmeasurable. Films cast at 2000 RPM had a thickness of approximately 65 nm (as measured by a profilometer) and were able to attain resonance in the QCM. With the PEDOT:PSS coated sensors, we were able to measure water uptake of the polymer film.

After verifying the water uptake of PEDOT:PSS films, the humidity setup was modified to reduce the pressure changes and to increase the humidity in the wet line. A schematic of the setup is illustrated in Figure 2. In this setup, the two nitrogen lines split from a single source, which sets the pressure in the system. The lines split via a three-way mixing valve, which has a handle to vary the amount of nitrogen diverted to the wet line or the dry line. The pressure is further stabilized by flow valves on the dry and wet lines. The wet line was also outfitted with a sintered glass outlet, which creates many small bubbles of nitrogen that then pass through a reservoir of water. This change increased the maximum attainable humidity of the system to approximately 98 %. Figure 20 below indicates the improvements in pressure stability in the system as measured by the QCM when the humidity of the system was changed. On the left was the original setup, where the flows to the nitrogen wet and dry lines had to be adjusted. On the right is the current setup, where the

total nitrogen flow is constant, but is diverted to the wet/dry lines. The system has much smaller pressure changes with the current setup, deconvoluting pressure changes from humidity changes.

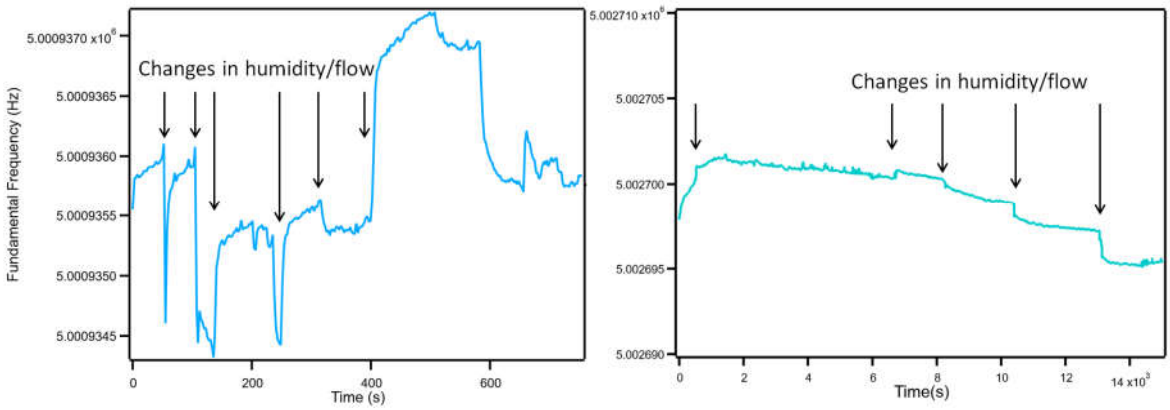

Figure 20: Comparison of the first humidity setup to the most recent revision (schematic in Figure 2). The new system has much smaller changes in flow rate per humidity change, leading to smaller "jumps" in the data.

The water uptake of PEDOT:PSS agrees with previous studies, confirming the accuracy of our QCM instrument (Figure 21)[1]. After the PEDOT:PSS films performed successfully in the QCM, we returned to testing the P($g_4$2T-T) films. In order to get a thick and uniform enough P($g_4$2T-T) film, the crystals were spun cast at 500 RPM and dried on a 100 °C hot plate for 10 minutes. Then, the films were dried overnight in the high vacuum oven. Samples were first equilibrated with dry N_2, as the baseline of the measurement tends to drift with time, as illustrated in Figure 22 as the Sauerbrey mass of the film drops below zero. This behavior is consistent with other QCM measurements and can be accounted for with a simple baseline shift. This film absorbed water readily, up to 1.046 µg/cm^2, when exposed to 98 % RH nitrogen. Given an approximate working area of 3.14 cm^2, the ~ 40 nm film absorbed ~ 3.3 µg of water. Future studies of the water uptake of P($g_4$2T-T) will more accurately measure the water uptake per gram of material and perhaps even per polymer

chain. Moreover, the development of a doping chamber that incorporates the QCM will allow users to evaluate the exact mass of dopant that enters P($g_4$2T-T) films, allowing for a precise measurement of dopant loading in the system.

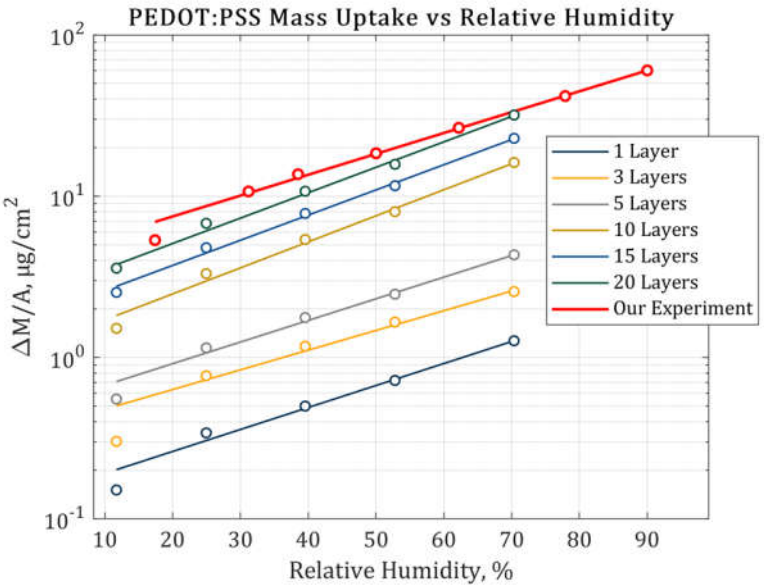

Figure 21: Water uptake of PEDOT:PSS, from (12) and compared to our results. These results match the proposed exponential trend from (12) within one standard deviation. Figure reproduced with permission from Phong Nguyen.

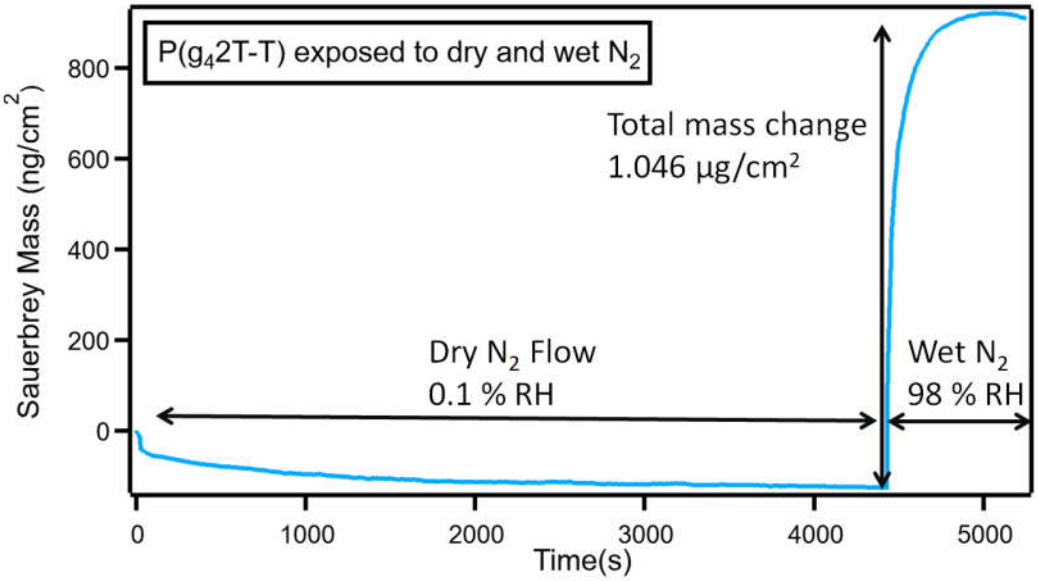

Figure 22: Example of mass uptake of P($g_4$2T-T) when exposed to humid air.

Conclusions and Future Work

The conjugated polymers ProDOT and P($g_4$2T-T) were characterized using a variety of methods to better understand the structure-property relationships that govern the behavior of these polymers. Polymer samples were doped with molecular dopants in order to induce electrical and ionic conduction, and then the polymers were studied using a variety of measurements including UV-Vis spectroscopy, DC conductivity, impedance spectroscopy, x-ray scattering, and QCM mass uptake measurements. Due to limited supply of ProDOT, P($g_4$2T-T) was the more heavily studied polymer of the two.

The two polymers, being similar in structure, exhibited similar behavior for the characteristics studied. Upon doping, both polymers exhibited electrochromism, as expected, and both developed polarons of the same energy in the IR region, indicating a similar energy state post-doping. Due to the dopant used (HTFSI), the dopant concentration in the films was not quantifiable by spectroscopic means, though the polymers were pushed to full bleaching. Post doping, films were subjected to DC conductivity tests. DC conductivity only yielded insight into the electronic conductivity of the films, which was very low and close to the noise levels of the instruments. This prompted the use of EIS on IDEs in order to obtain film ion and electron conductivity.

The ProDOT samples doped with ionic salts exhibited mixed conduction, and the films doped with molecular dopants like F_4TCNQ predictably only exhibited electronic conduction. Notably, the experimental noise was greatly reduced by the use of IDEs; however, the IDEs also tended to induce capacitive phase element-like behavior in the films, which manifests as a depressed semicircle in the Nyquist plot. This behavior was also reflected in the EIS of P($g_4$2T-T). Using EIS, it was found that the P($g_4$2T-T) sample was

likely already oxidatively doped before use, so its "pristine" conductivity was not much different from the doped conductivity. Moreover, the polymer was not as insulating in the pristine case as reported in previous works, and was not as conductive in the doped case as reported in previous works. P($g_4$2T-T) did not exhibit ionic conduction in EIS, perhaps because the electronic signal overwhelmed the ionic signal in the film. If the film was de-doped, then doped with an ionic salt, the ionic conduction may be detectable by EIS.

Upon doping, both ProDOT and P($g_4$2T-T) experience structural changes, as measured by GIWAXS. ProDOT appears to reorganize into cylindrical rods that are hexagonally packed when doped with HTFSI. Perhaps the dopant stabilizes the polymer in such a configuration by $TFSI^-$ residing in the sidechains of the polymer. P($g_4$2T-T) also exhibits drastic structural changes upon doping, notably an enhancement in molecular packing order along the alkyl direction. In P($g_4$2T-T) films, the molecular reordering is typically reduced when the film is doped then hydrated, and the film loses most of its ordering when it is hydrated, then doped. Thermal annealing of the films accentuates the changes in molecular ordering after doping, in addition to removing excess dopant on the surface of the film.

The amount of water uptake of the films was only measured for P($g_4$2T-T), as the ProDOT polymer supply had run out. After much calibration difficulty with the QCM, it was found that films on the order of 40-100 nm in thickness are the most easily measured by the Gamry QCM. Under these conditions, the setup is capable of reproducing previous water uptake measurements of PEDOT:PSS. This gives us confidence that the QCM is measuring mass accurately. A thin film of P($g_4$2T-T) was found to uptake ~ 3.3 μg of water. The mass of the film was not measured before the water uptake measurement, so it is difficult to

ascertain the water uptake per mass of film. This is a key area of study in the future, to better understand the ability of films to uptake both water and dopant under various conditions.

Further work remains to fully characterize these polymers and to understand the mechanisms that govern ion and electron transport in the polymer films. First, the P($g_4$2T-T) polymer must be chemically de-doped in order to reproduce and verify previous experiments. Returning the polymer to a true pristine state will enhance the structural and electronic changes upon doping and upon humidification. Next steps also include developing a doping chamber to be used in conjunction with the QCM. This will enable the measurement of dopant uptake in a film when spectroscopic techniques such as UV-Vis cannot measure the dopant concentration, as is the case for the dopant HTFSI. The fine tuning of humidity and dopant concentration of a thin film of P($g_4$2T-T) will allow researchers to optimize conditions for ion and electron conduction in those films. A strict comparison of ProDOT to P($g_4$2T-T) across structure, conductivity, and water/dopant uptake would be helpful towards increasing understanding of the role of the solubilizing ethylene glycol sidechains. While it is generally understood that PEG sidechains increase the solubility of the polymers, comparing the two polymers, which have similar backbones but different ratios of PEG sidechains to monomer units, would be illuminating.

The continued study of mixed ion-electron conductors will open the doors for novel technological applications, especially in the field of wearables and implantable sensors. Once design rules are established for MIEC polymers, we may witness a rapid adoption of this technology into real devices that interface the electronic with the biological.

References

1. Jaruwongrungsee, K. *et al.* High-sensitivity humidity sensor utilizing PEDOT/PSS printed quartz crystal microbalance. in *The 8th Electrical Engineering/ Electronics, Computer, Telecommunications and Information Technology (ECTI) Association of Thailand - Conference 2011* 66–69 (2011). doi:10.1109/ECTICON.2011.5947772.

2. Mazaheripour, A., Thomas, E. M., Segalman, R. A. & Chabinyc, M. L. Nonaggregating Doped Polymers Based on Poly(3,4-Propylenedioxythiophene). *Macromolecules* **52**, 2203–2213 (2019).

3. Ion Electron–Coupled Functionality in Materials and Devices Based on Conjugated Polymers - Berggren - - Advanced Materials - Wiley Online Library. https://onlinelibrary.wiley.com/doi/full/10.1002/adma.201805813.

4. Noriega, R. *et al.* A general relationship between disorder, aggregation and charge transport in conjugated polymers. *Nature Materials* **12**, 1038–1044 (2013).

5. Cheng, F. & Ratner, D. M. Glycosylated Self-Assembled Monolayers for Arrays and Surface Analysis. *Methods Mol Biol* **808**, (2012).

6. *eQCM-I Mini User Manual*. vol. 1 (MicroVacuum Ltd, 2018).

7. Sharon, D. *et al.* Interrogation of Electrochemical Properties of Polymer Electrolyte Thin Films with Interdigitated Electrodes. *Journal of The Electrochemical Society* **165**, H1028–H1039 (2018).

8. Thomas, E. M., Davidson, E. C., Katsumata, R., Segalman, R. A. & Chabinyc, M. L. Branched Side Chains Govern Counterion Position and Doping Mechanism in Conjugated Polythiophenes. *ACS Macro Lett.* **7**, 1492–1497 (2018).

9. Lim, E., Peterson, K. A., Su, G. M. & Chabinyc, M. L. Thermoelectric Properties of Poly(3-hexylthiophene) (P3HT) Doped with 2,3,5,6-Tetrafluoro-7,7,8,8-tetracyanoquinodimethane (F_4TCNQ) by Vapor-Phase Infiltration. *Chemistry of Materials* **30**, 998–1010 (2018).

10. Patel, S. N., Javier, A. E., Stone, G. M., Mullin, S. A. & Balsara, N. P. Simultaneous Conduction of Electronic Charge and Lithium Ions in Block Copolymers. *ACS Nano* **6**, 1589–1600 (2012).

11. Kroon, R. *et al.* Polar Side Chains Enhance Processability, Electrical Conductivity, and Thermal Stability of a Molecularly p-Doped Polythiophene. *Advanced Materials* **29**, 1700930 (2017).

12. The Constant Phase Element. http://www.consultrsr.net/resources/eis/cpe1.htm.

13. Kiefer, D. *et al.* Double doping of conjugated polymers with monomer molecular dopants. *Nature Materials* **18**, 149–155 (2019).

14. Chang, W. B. *et al.* Electrochemical Effects in Thermoelectric Polymers. *ACS Macro Letters* **5**, 455–459 (2016).

15. Mazaheripour, A., Thomas, E. M. & Segalman, R. A. Doping-Induced Structural Order in Non-Aggregating Conductive Polythiophenes. 30.